Annals of Biomedical Engineering, Vol. 41, No. 8, August 2013 (© 2012) pp. 1646–1660
DOI: 10.1007/s10439-012-0646-9

Adaptive Fractal Analysis Reveals Limits to Fractal Scaling in Center of Pressure Trajectories

NIKITA KUZNETSOV,[1] SCOTT BONNETTE,[1] JIANBO GAO,[2,3] and MICHAEL A. RILEY[1]

[1]Center for Cognition, Action, & Perception, Department of Psychology, University of Cincinnati, Cincinnati, OH 45221-0376, USA; [2]PMB Intelligence, LLC, West Lafayette, IN, USA; and [3]BME, School of Life Sciences & Technology, Xi'an Jiaotong University, Xi'an 710049, People's Republic of China

(*Received 31 March 2012; accepted 22 August 2012; published online 7 September 2012*)

Associate Editor Thurmon E. Lockhart oversaw the review of this article.

Abstract—Fractal time series analysis methods are commonly used for analyzing center of pressure (COP) signals with the goal of revealing the underlying neuromuscular processes for upright stance control. The use of fractal methods is often coupled with the assumption that the COP is an instance of fractional Gaussian noise (fGn) or fractional Brownian motion (fBm). Our purpose was to evaluate the applicability of the fGn–fBm framework to the COP in light of several characteristics of COP signals revealed by a new method, adaptive fractal analysis (AFA). AFA quantifies how the variance of the residuals to fits of a globally smooth trend signal scales with the time scale at which the fits are performed. Application of AFA to COP signals revealed that there are potentially three fractal scaling regions in the COP as opposed to one as expected from a pure fGn or fBm process. The scaling region at the fastest scale was anti-persistent and spanned ~30–90 ms, the intermediate was persistent and spanned ~200 ms–1.9 s, and the slowest was anti-persistent and spanned ~5–40 s. The intermediate fractal scaling region was the most clearly defined, but it only contributed around 11% of the total spectral energy of the COP signal, indicating that other features of the COP signal contribute more importantly to the overall dynamics. Also, more than half of the Hurst exponents estimated for the intermediate region were greater than the theoretically expected range [0,1] for fGn–fBm processes. These results suggest the fGn–fBm framework is not appropriate for modeling COP signals. ON–OFF intermittency might provide a better modeling framework for the COP, and multiscale approaches may be more appropriate for analyzing COP data.

Keywords—Nonlinear analysis, Detrended fluctuation analysis, Adaptive fractal analysis, Postural control, Fractal scaling, Center of pressure.

Address correspondence to Michael A. Riley, Center for Cognition, Action, & Perception, Department of Psychology, University of Cincinnati, Cincinnati, OH 45221-0376, USA. Electronic mail: michael.riley@uc.edu

INTRODUCTION

Upright, bipedal stance in humans is achieved through a set of complex and interactive neural, sensory, and musculo-skeletal processes that are shaped by task and environmental contexts. The fundamental mechanisms of postural control remain incompletely understood. Many efforts to understand these mechanisms focus on the analysis of postural sway, the continuous variation in the position of the body's center of mass. Postural sway during quiet stance is often operationalized in terms of center of pressure (COP) trajectories measured using a force platform. The COP is the average location of the ground reaction force vector. COP displacements correlate highly with center of mass displacements during quiet stance.[34] COP trajectories (Fig. 1) are highly variable, typically nonstationary (e.g., the mean or variance is time-dependent), and complex.[29]

Rather than just reflecting unsystematic noise, complex patterns of movement variability are important for understanding motor coordination and control.[6,18,30,33] In the study of posture and balance, specifically, the structure of variability of COP trajectories may contain valuable clues about the underlying organization of postural control.[30] Accordingly, many nonlinear time series methods have been used to analyze COP trajectories, including recurrence quantification analysis,[29] several types of fractal methods,[4,8,10,28] and entropy measures.[15] The goals of applying these analyses have included identifying basic balance mechanisms, uncovering age-related changes in normal balance, discovering signatures of balance and movement pathologies, and revealing mechanisms of expertise and the effects of training.

Fractal methods have gained widespread acceptance for characterizing COP signals. Their use was

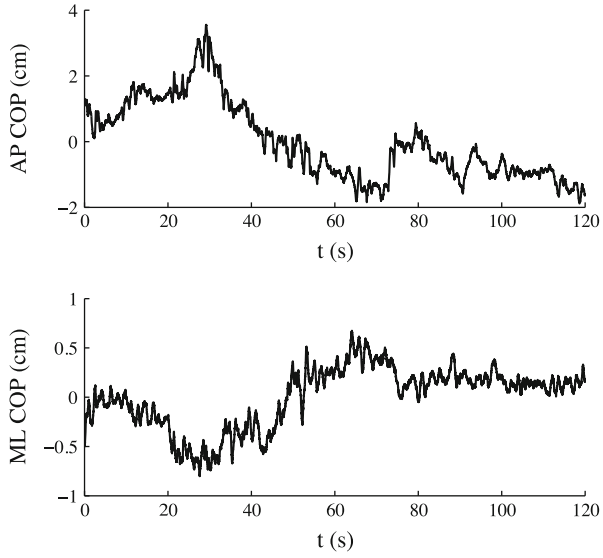

FIGURE 1. Sample center of pressure (COP) time series recorded from a force platform. The COP is the average location of the ground reaction force vector, and its fluctuations are closely related to center of mass fluctuations during quiet stance. The COP is a commonly used measure of global postural activity. The top panel shows AP COP motion and the bottom panel shows ML COP motion. Characterizing the time-varying properties of the COP is an important goal, but a challenging one in light of the complexity and nonstationarity of COP signals. Note that the top and bottom panels are on different scales; we zoomed in on the ML signal (ML COP signals typically have lower amplitude than AP COP signals) to better reveal the character of the signal.

motivated initially by work that questioned interpretations of COP fluctuations as deterministic chaos in favor of a stochastic approach based on "colored" noise processes—noise processes that are not completely random but that instead contain subtle forms of structure.[5] Additional research confirmed that COP signals have a noisy, but not completely random, temporal structure.[30] Fractal methods appear highly suitable for stochastic signals such as these.

Specifically, Collins and DeLuca[5] identified COP signals as a particular type of stochastic process termed *fractional Brownian motion* (fBm),[24] which is a Gaussian process having zero mean, a power-law increasing variance (t^{2H}), and power-law decaying spectral density ($1/f^{2H+1}$). fBm is a special type of nonstationary long-memory process.[2] The degree and nature of "memory" in the signal (autocorrelation structure that represents a departure from a purely random process) is indexed by the Hurst exponent, H, where $H = 0.5$ indicates a random or short-memory process, $0 < H < 0.5$ indicates a negatively correlated (anti-persistent) process, and $0.5 < H < 1$ indicates a positively correlated (persistent) long-memory process. The increments of an fBm process form a stationary *fractional Gaussian noise* (fGn) process. Familiar noise processes such as brown noise and white noise respectively exemplify fBm and fGn. Figure 2 depicts fBm and fGn.

Several previous studies that analyzed COP signals with fractal methods have produced findings that are inconsistent with what would be expected from the fGn–fBm framework. One inconsistency regards the number of scaling regions exhibited by COP signals. Pure fGn or fBm processes should exhibit a single regime of linear scaling. Early findings using stabilogram diffusion analysis instead revealed two (or more) distinct scaling regions with a cross-over between persistent and anti-persistent COP fluctuations.[4,13,28] Delignières *et al.*[8] first attributed this finding to what they considered to be a methodological shortcoming of stabilogram diffusion analysis, which does not include integration as a pre-processing step.[7,8] Consistent with their claim, later studies that used detrended fluctuation analysis (DFA)[27] on integrated COP signals reported a single scaling region.[8,10] However, this issue has not yet been resolved, because several other studies found two scaling regions even for integrated COP signals,[3,26] leaving open the question of whether the fractal scaling exhibited by the COP is consistent with pure fBm.

In response to the question of multiple scaling regions in COP data and other types of time series, Bardet and Bertrand[1] presented a multiscale-fBm model (i.e., fBm with multiple scaling regions that exhibit distinct slopes). They also presented a wavelet-based method for estimating H and the critical time scales at which occur the inflection points that separate scaling regions. This generalization of the fGn–fBm framework is potentially useful in that it can account for the presence of multiple scaling regions. However, as described in the following paragraphs, COP data nevertheless exhibit additional properties that remain inconsistent with even this generalized, multiscale-fBm framework.

A second and related inconsistency (see Table 1 in Delignières *et al.*[7]) is that the slopes used to estimate the values for non-integrated and integrated COP signals do not differ by the theoretically expected value of 1.[12,14] A fBm process can be obtained by integrating a fGn process (by definition they are related *via* an integration-differentiation relation), so the difference in the slopes of the fits for two such signals should differ by exactly 1 (see Fig. 2, bottom panels).[11,12] For COP signals, however, the difference is usually less than 1. This under-additivity provides further indication that the fGn–fBm framework should not be applied to COP signals.

The theoretical upper-limit of H for fGn and fBm processes is, by mathematical definition, $H = 1$.

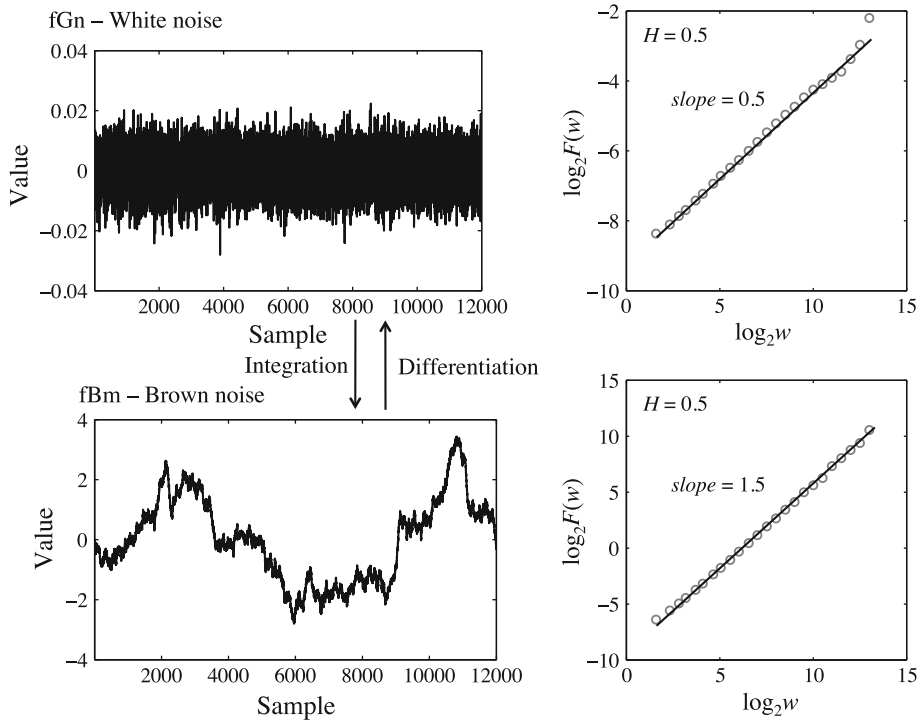

FIGURE 2. Top: A time series (left) of white noise, a fGn process, and (right) its corresponding AFA plot (these plots are described in detail later in the text). Bottom: A time series (left) of brown noise, a fBm process, and (right) its corresponding AFA plot. The two processes are related; fGn is an increment series and its integration yields a random walk process, fBm. The slope of the linear fit on a log–log AFA plot is 0.5 for white noise (corresponding to $H = 0.5$), indicating a random, uncorrelated process. The slope for the brown noise is 1.5, indicating a persistent (positively correlated) process. Both time series were integrated prior to AFA because the analysis was developed for fBm-like processes. Integrating an fBm process increases the slope by 1 as shown in the AFA plot of the simulated fBm process (bottom right panel). To obtain the Hurst exponent of the original non-integrated data in this case, one needs to subtract 1 from the slope of the fitted line ($H = 0.5$).

TABLE 1. Characteristics of the linear fits to the AFA curves of nonintegrated COP data.

	Fast	Intermediate	Slow
AP			
H (*SD*)	0.22 (0.07)	1.04 (0.15)	0.27 (0.13)
Beginning (*SD*)	30 ms (0)	149 ms (67)	5.37 s (2.78)
End (*SD*)	87 ms (24)	1.91 s (0.98)	37.15 s (6.24)
N	39	115	115
ML			
H (*SD*)	0.21 (0.04)	1.00 (0.10)	0.17 (0.06)
Beginning (*SD*)	30 ms (0)	238 ms (92)	5.19 s (1.52)
End (*SD*)	98 ms (32)	1.84 s (0.54)	38.75 s (4.31)
N	92	115	115

Note. N is the number of times we observed the scaling region. We analyzed a total of 120 AP and 120 ML COP time series. The end and the beginning of the intermediate scaling region are presented in units of ms. The end of the intermediate scaling region and slow region are presented in units of seconds.

Processes with $H > 1$, which are not only possible but abundant,[12,14] do not fall within the fGn or fBm framework, but instead are different classes of signals altogether. COP signals often have $H > 1$, as we show in our results later, thus pointing to a third inconsistency that raises questions about the suitability of the fGn–fBm framework (including the generalization to multi-scale fBm) and points instead toward other types of processes as providing a modeling and analysis framework for the COP. Hurst exponents that exceed 1 can come from processes such as ON/OFF intermittency, Lévy processes, auto-regressive models, and other nonstationary processes; these may provide a more suitable framework for modeling and characterizing COP signals and postural control, more generally.

The above-mentioned considerations thus raise some fundamental questions about fractal analysis of COP signals. Prominent among these questions are (1) whether or not the fGn–fBm framework within which DFA and other fractal analysis methods have been developed[11] applies to COP signals, (2) whether COP signals exhibit one or multiple fractal scaling regions, and perhaps most importantly, (3) which aspects of postural variability are captured by fractal analyses. The last point regards the amount of contribution of any identified fractal dynamics to the overall signal. Previous work has shown that in some cases even when fractal scaling is present it may only contribute a relatively small amount of the spectral energy to the

overall signal.[15] These issues are important for developing models of normal and pathological postural control, and for guiding the use of analysis methods for quantifying postural stability and performance.

To address the above fundamental issues, in this paper we analyze COP signals using *adaptive fractal analysis* (AFA).[13,17,19] AFA is a relatively new fractal method that has not yet been widely used for analysis of COP signals. Presently, DFA is perhaps the most commonly used fractal method for analyzing COP. DFA is preferred over many other fractal methods since H estimated by many other fractal analysis methods (but not DFA) saturate at 1, while as noted COP signals may have $H > 1$. Also, DFA characterizations of COP signals have been found to be reliable over repeated test sessions.[20]

However, prior work has shown that AFA has a number of advantages over DFA: (1) DFA involves linear fitting to non-overlapping segments of a signal, with discontinuities or even large, abrupt jumps at the boundary of the segments, while AFA identifies a global smooth trend, which is obtained by optimally combining local linear or polynomial fitting; (2) AFA can deal with arbitrary, strong nonlinear trends while DFA cannot[13]; (3) AFA has better resolution of fractal scaling behavior for short time series data[16]; and (4) AFA has a direct interpretation in terms of spectral energy,[13] while DFA does not (we present the details of the analysis in the Materials and Methods section). These attributes of AFA are important for resolving the previously described issues about how to best characterize and model COP signals.

Resolving these issues also requires some additional methodological development that we have begun to undertake in this paper. In many situations fractal scaling may be limited to a finite range of time scales, but this may not be considered when quantifying H in practice. Identifying linear scaling regions can be a challenging issue, and misidentification of them can lead to considerable inaccuracies in the estimation of H. We therefore present in this paper some objective model-selection methods for identifying scaling regions. While it is desirable to make these methods as automated and objective as possible, as we will show, it nevertheless remains important to visually inspect the data to ensure that any fractal scaling regions that are numerically identified are indeed legitimate.

The main purpose of this paper was to examine whether the fGn–fBm framework is appropriate to apply to COP signals. We pursued this question from three angles. First, we developed a semi-automated model-selection algorithm to identify scaling regions to objectively identify how many fractal scaling regions there are in the COP signal. Second, we determined the amount of spectral energy contributed to the signal from each of the identified scaling regions. Third, we determined how many of the scaling exponents exceeded the maximum value ($H = 1$) theoretically expected from an ideal fGn–fBm process.

MATERIALS AND METHODS

Subjects

Forty undergraduate students from the University of Cincinnati (28 women, 12 men) participated in exchange for course credit. Their ages ranged from 18 to 33 years, with a mean of 19.90 years ($SD =$ 2.66 years). All had normal or corrected-to-normal vision, and none reported an injury or neurological or balance impairment at the time of the experiment. All participants gave informed consent and all procedures were IRB-approved.

Apparatus and Procedure

There were three trials, each lasting 2 min. During each trial subjects were instructed to stand naturally and comfortably and to focus their vision at a single location on a uniformly white wall 1 m away. Subjects stood atop an AccuSway + force platform (AMTI, Watertown, MA). For each trial we obtained from the force platform recordings the COP in the anterior-posterior (AP) and medial-lateral (ML) directions at a sampling rate of 100 Hz. (It should be noted that 100 Hz is probably the upper limit for a choice of sampling rate for COP data, and typically a lower rate (25–50 Hz) is sufficient and could be preferred in order to avoid artifacts associated with oversampling that can occur with many analysis methods. AFA is unlikely to be affected by such artifacts, but sampling rate will affect the resolution of the analysis. We return to this issue in the Discussion.) This yielded 6 time series for each participant. After the data were truncated to exclude the first 5 s of the trial (yielding final time series of 11,500 samples), AFA was performed on each individual's time series in both AP and ML directions.

Adaptive Fractal Analysis

Like DFA, AFA begins with a pre-processing stage of integrating the data if the data are akin to an increment process but not if they are akin to a random-walk process. As an example of the difference between these, fGn is an increment process and fBm is a random-walk process (see Fig. 2). The former is stationary, noisy and irregular, while the latter appear nonstationary and though they are still irregular they have an overall smoother appearance. Visual

inspection revealed that the current COP signals were more like fBm (compare Figs. 1 and 2), so we did not integrate them. Visual inspection and careful exploration of one's dataset prior to any fractal analysis is important and should be done prior to any quantitative analysis.[14,23]

Working then from the truncated time series, which we denote $u(i)$, the next step is to determine a global trend $v(i)$, $i = 1, 2,\ldots,N$, where N is the length of the process $u(i)$.[17,32] This is achieved by partitioning $u(i)$ into windows of size $w = 2n + 1$, with lengths overlapping by $n + 1$ points (since setting w determines the value of n, n is not a free parameter that must be chosen). Within each window the best fitting polynomial y of order M (in our case $M = 1$) is fit to the data. The combined fit $y^{(c)}$ (where c indicates "combined") to the overlapping regions is a weighted combination of the fit of the two adjacent regions i and $i + 1$ (i.e., $y^{(i)}$ and $y^{(i+1)}$) to ensure that the concatenation of local fits is smooth [i.e., that $v(i)$ is continuous and differentiable], according to

$$y^{(c)}(l) = w_1 y^{(i)}(l+n) + w_2 y^{(i+1)}(l), \quad l = 1, 2, \ldots, n+1, \tag{1}$$

where $w_1 = \left(1 - \frac{l-n}{n}\right)$ and $w_2 = \frac{l-1}{n}$. By choosing the parameters of each local fit to maximize the goodness of fit in each case, and then applying Eq. (1) to stitch the local fits together, the global fit will be the best (smoothest) fit to the overall time series. Note that because of the stitching even when $M = 1$ is selected the global trend signal will end up being curved even though the local fits are linear.

Then, the residual of the fit, $u(i) - v(i)$, is computed. The variance of the residual yields the Hurst exponent H, which scales with window size w according to

$$F(w) = \left[\frac{1}{N}\sum_{i=1}^{N}\left(u(i) - v(i)\right)^2\right]^{1/2} \sim w^H, \tag{2}$$

Thus, by performing the fits and computing the residual and its variance for each window size w, and then plotting $\log_2 F(w)$ as a function of $\log_2 w$ (see Fig. 3 for a visual description of the method, and Fig. 2, right, for complete plots), the presence of fractal scaling can be identified as a linear relation in the plot, with the slope of this relation providing the estimate of H. For the results reported below, we used a step size of 0.5 $\log_2 w$ and polynomial fitting of order $M = 1$.

Working from a plot of $\log_2 F(w)$ as a function of $\log_2 w$, one must determine whether fractal scaling is present and whether it is present in one or more regions of the plot. We first visually inspected every individual AFA plot of the COP data to evaluate the presence of fractal scaling and the number of possible linear scaling regions in these data. Visual inspection suggested that in most cases there were either 2 or 3 scaling regions present at relatively fast (only for three scaling region cases), intermediate, and slow time scales. However, we wanted to make sure that we did not arbitrarily assign a 2 or 3 region model to the data just based on visual inspection. Accordingly, we created a model fitting routine that allowed us to compare the goodness of fit of these two model types using a formal procedure of model selection based on the small-sample Bayesian information criterion (SICc) which penalizes the increased goodness of fit as additional parameters are added to the model.[25] For each trial, we first fitted 2- and 3-region piecewise linear models, then obtained a SICc value for each of the fits, and then chose the model with the lower value of SICc. We used that model to estimate H and the boundaries of the scaling regions for each trial.

For the 2-region models, we fitted the following piecewise linear model with two regions and one breakpoint at $\log_2 w = k$ between them to the AFA curves

$$\begin{aligned} y &= b_1 x + a_1 \quad \text{for } x < k, \\ y &= b_2 x + a_2 \quad \text{for } x > k. \end{aligned} \tag{3}$$

In order to choose the best 2-region model, we evaluated the global goodness of fit for all two-region fits and all possible breakpoint locations between $\log_2 w$ values from 5 to 80% of all $\log_2 w$. The reason for these particular cut off points was that the visible boundaries of the regions were typically within this range of window sizes. We allowed the fit to start at either the first or the second scaling region and allowed up to three $\log_2 w$ separation between the regions. This was done so that the fits were not constrained to continuous linear regions only. Goodness of fit was quantified as the residual sum of squares (RSS),

$$\text{RSS} = \sum (y_i - \hat{y})^2. \tag{4}$$

After iteratively fitting the defined 2-region models, we found the 10 best-fitting models and then chose the one with the longest first region. We prioritized the identification of the first scaling region because it seemed to be the most reliable, clearly defined, and longest scaling region based on the preliminary visual inspection of all time series.

The 3-region model was defined by adding another breakpoint,

$$\begin{aligned} y &= b_1 x + a_1 \quad \text{for } x < k_1, \\ y &= b_2 x + a_2 \quad \text{for } k_1 < x < k_2, \\ y &= b_3 x + a_3 \quad \text{for } x > k_2. \end{aligned} \tag{5}$$

The presence of two breakpoints required a more elaborate procedure for evaluating fits of the 3-region

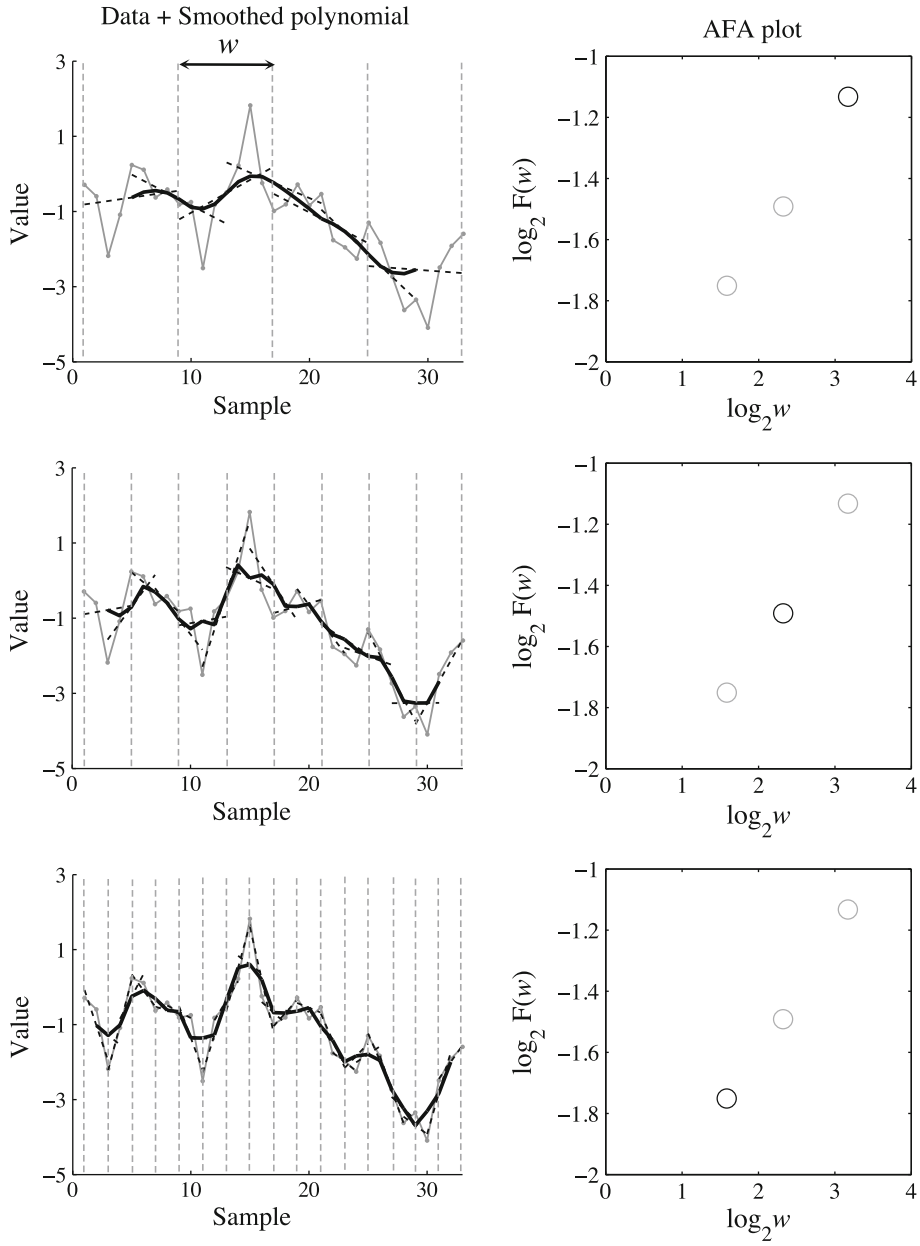

FIGURE 3. The figure provides a visual illustration of the steps of the AFA. First, polynomials of order *M* are fit to the time series using windows of size *w* overlapping by a half-window size (for visual clarity we depicted only non-overlapping windows). We plotted first-order polynomial fits (dashed) over the simulated time series (shown in light grey). The black line is the smoothed fit between the adjacent overlapping polynomial fits that is obtained by weighted averaging using the weighting function as described by Eq. (1) in the text. Lastly, the right panels show a $\log_2$–$\log_2$ plot of the amount of variability, *F*(*w*), of the original data around the smoothed fit (black line). The presence of fractal scaling is assessed from linear regions in the log–log AFA plot (see text for details).

models than for the 2-region models. We first created all possible combinations of non-overlapping region boundaries to be evaluated for the fit (e.g., region 1 ranging from $1 \le \log_2 w \le 2$, region 2 from $3 \le \log_2 w \le 5$, and region 3 from $5 \le \log_2 w \le 7$). The combinations were then limited by the criteria that (a) the intermediate region should be longer than $3 \log_2 w$ steps (as suggested by visual inspection of the plots), (b) the first (fast) region starts at the first considered w ($2^{1.58}$ samples or ~30 ms), (c) the last (slow) region ends at maximum w (2^{12} samples or 40.96 s), and (d) the distance between adjacent regions should be less than 4 $\log_2 w$. Next, we iteratively fitted the 3-region models while evaluating the RSS for each fit. We then identified the 10 models with the smallest RSS and chose the one with the longest intermediate scaling region.

Typically many good-fitting models had similar RSS values, so this step was warranted given our priority to find the model with the longest intermediate scaling region. We prioritized the identification of the intermediate scaling region for the 3-region model (this corresponded to the first scaling region for the 2-region model above) because these regions seemed to be the most reliable, clearly defined, and longest scaling regions based on the preliminary visual inspection of all time series.

After finding the fits of each model, we used the SICc criterion to choose between the 2-region and 3-region models. SICc was defined using the formula[25]:

$$\mathrm{SICc} = \ln\left(\frac{\mathrm{RSS}}{S}\right) + \frac{p\ln(S)}{S-p-2}, \qquad (6)$$

where S is the number of fitted scales, RSS is the residual sum of squares, and p is the number of model parameters.[31] For the 2-region model we set p to 6 (starting position, breakpoint, and the two slopes and intercepts) and for the 3-region model p was set to 8 (two breakpoints, three sets of two slopes and intercepts). We used the starting position as a parameter in the 2-region model because even in the cases where two regions were a good fit there still was typically one initial point hinting at the fast scaling region, and such points otherwise could have influenced the fitting and selection procedures. This was not necessary for the 3-region model, where two breakpoint parameters were used instead. We chose the model with the lowest SICc from the best-fitting (lowest RSS) 2- and 3-model fits and calculated the slopes (i.e., H), intercepts, and boundaries for each region in this model.

We started with a total of 240 COP time series (120 AP and 120 ML) and fitted the three- and two-region models to their AFA curves. A total of 6 COP time series in the AP plane (~2.5% of the data) were selected to have a 2-region fit according to our model selection procedure. An example of one of these AP COP recordings is shown in panel A of Fig. 4. However, we later refitted those 6 AP COP trials with the 3-region model because it was the dominant model form identified in our data set. We then performed another visual inspection of each fit to ensure that the fits were not biased or otherwise influenced by some anomalous feature in the data. For the majority of time series the selected model accorded with the appearance of the plot. However, five AP COP series appeared to have four scaling regions in their AFA plots instead of three (see an example in panel B of Fig. 4), with the fourth appearing at relatively long time scales. Those trials were similarly refitted with a three-region model including only the first three scaling regions and disregarding the last one (which typically spanned the 4–5 largest $\log_2 w$ scales) because the dominant model had three regions. Panel C in Fig. 4 depicts a 3-region AFA plot pattern that was most frequent in the present data set.

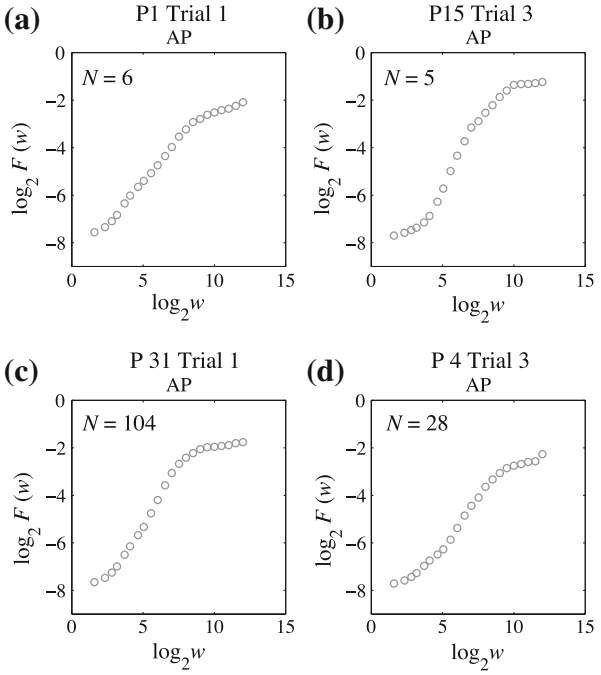

FIGURE 4. Examples of different AFA plots [$\log_2 F(w)$ as a function of $\log_2 w$] observed in our data set. Panel a shows an example of an AFA plot with two scaling regions (there were 6 AP recordings such as these). Panel b shows an example with four scaling regions (there were 5 AP recordings such as these). Panel c shows an example of the most frequently identified pattern with three linear scaling regions. Panel d depicts an example AFA plot with an outlying observation at the largest scale (there were 12 AP and 16 ML such recordings); these AFA plots were refitted with the same model fitting procedure disregarding the outlying observations.

We further excluded several trials (we removed both AP and ML series for those particular trials) from the analysis. One trial was excluded due to instrumentation error. We excluded one trial because the intermediate scaling region in the ML plane for that trial was very short—around four $\log_2 w$ scales—and the modeling routine could not fit that curve well. There were also three AP COP recordings that showed a curved slow scaling region; we removed these trials from the analysis because these regions were not well characterized by linear fits. After removing these five trials in total, the final number of analyzed time series was 230 (115 for each AP and ML).

Out of the total number of analyzed trials, 28 (~12% of the data, and 12 AP COP and 16 ML COP time series) showed singular anomalous departures from linear scaling at larger $\log_2 w$ values (see example in panel D of Fig. 4). These trials had to be refit with the same 3-region model automatically but

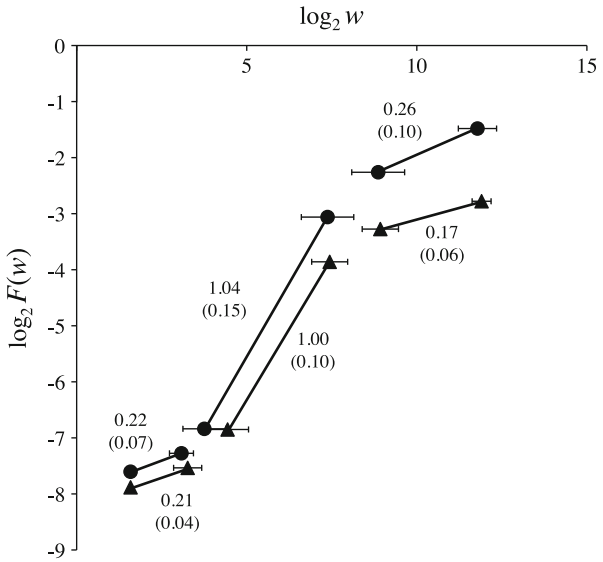

FIGURE 5. Results of AFA conducted on the AP and ML COP time series. The plot depicts the average linear fits to the short, intermediate, and long time scales of COP fluctuations (excluding trials for which a scaling region was deemed absent). Error bars represent the standard deviation of the $\log_2 w$ region boundaries observed across all participants and all trials. Linear fits were obtained with the three-region model fitting procedure described in the method section. Mean *H* are indicated for each region (*SD* in parentheses).

disregarding the smallest w scale and up to three of the largest w scales (mean = 1.53 scales, $SD = 0.69$). Additionally, in many cases (detailed below for AP and ML) the fast scaling region spanned only two points. Since a line can be defined between any two points, we did not consider these cases as instances of true scaling. We therefore did not include these data in any of the reported results, and we return to this issue in the Discussion. Out of all the trials analyzed, AP 6 trials showed only two scaling regions, 104 showed three scaling regions, and 5 showed four scaling regions, while for ML all 115 trials showed three scaling regions. The averaged results of the 3-region model fitting procedure for the whole dataset are shown in Fig. 5, and examples of the variety of data we encountered are in Fig. 6.

Spectral Analysis

After we identified the linear scaling regions and estimated the H for each one, we determined the amount of spectral energy associated with each of the regions. The rationale for this was to elucidate the contribution of the fractal dynamics of each scaling region to the COP signal; that is, we asked if any

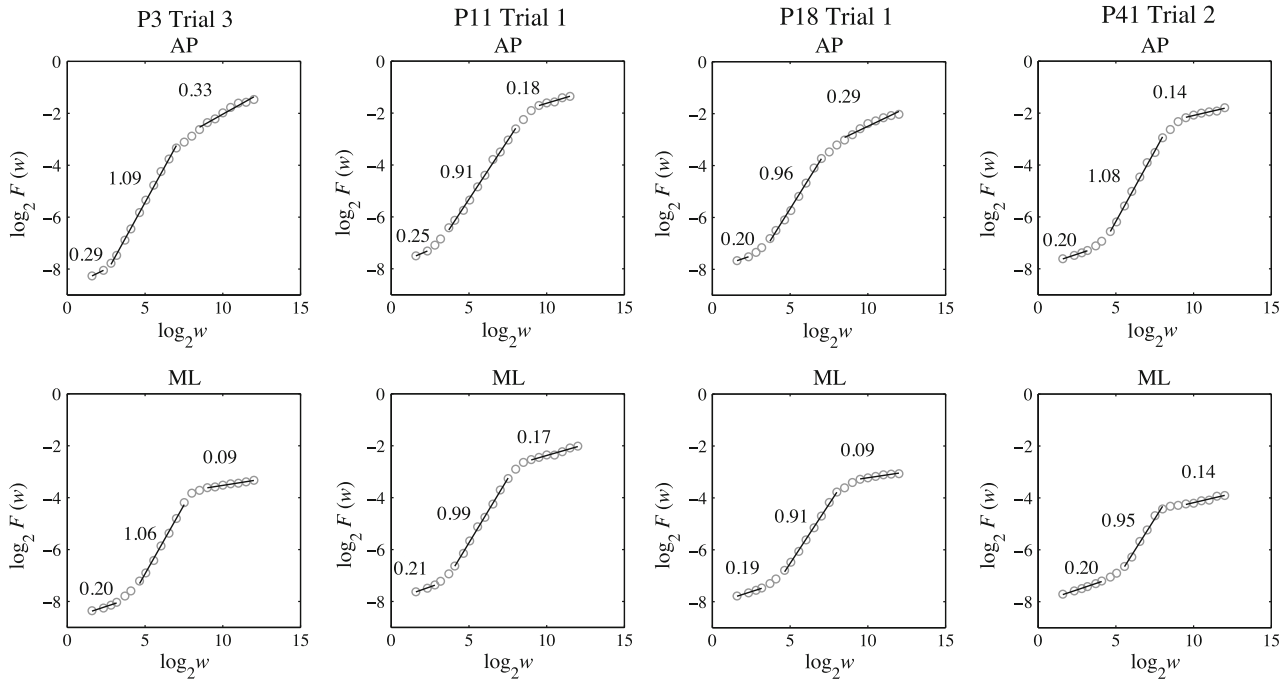

FIGURE 6. There was a variety of behaviors of scaling in the AFA plots in the AP and ML planes. All ML recordings showed fairly well-defined three-region scaling as illustrated in the bottom panels of the figure. In the AP plane, some trials showed relatively well-defined intermediate and large time scale regions, but did not show a clearly defined linear scaling at the smallest scale (P3 and P11). Several had relatively long small-scale regions (e.g., Participant 41). The fit in the largest scale was most variable and we also observed that for three participants the scaling function did not behave linearly (for example P18; these trials were excluded from the analysis). Participant 41's data showed three clear scaling regions.

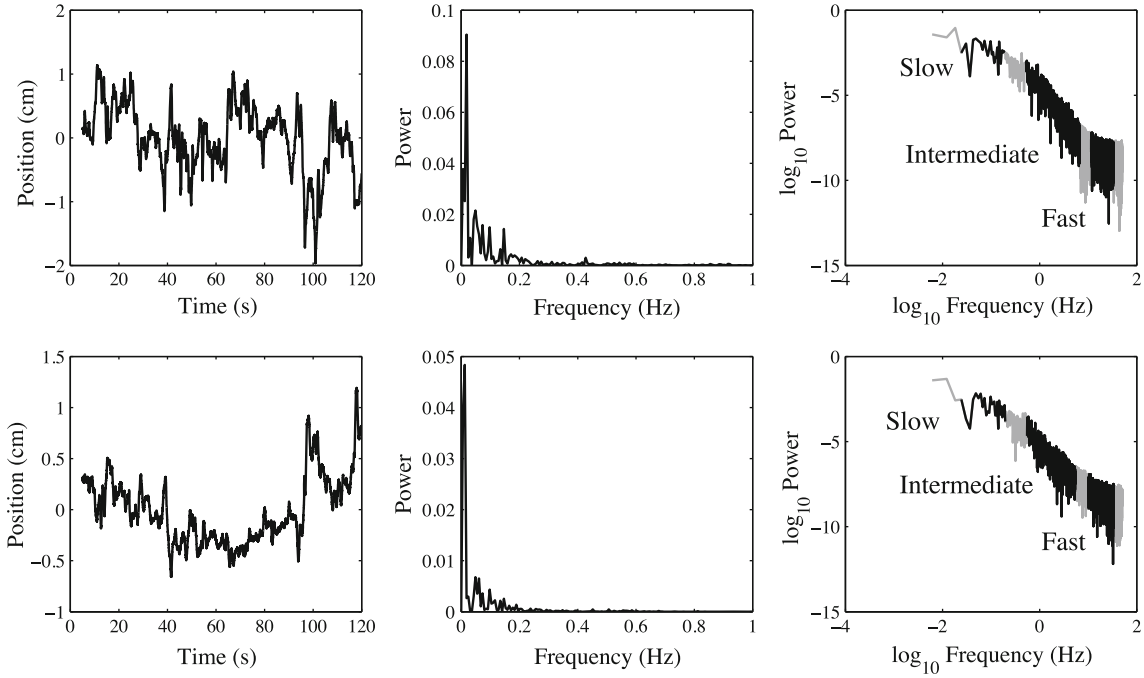

FIGURE 7. Power spectral density (PSD) plots for the AP and ML COP data. The left panels depict the raw, centered COP time series in the AP (top) and ML (bottom) planes. The central panels show the PSD of the same time series on linear axes to highlight that most of the power is visible in the lower frequencies of the COP signals. The panels on the right show the same PSD in log–log coordinates. We darkened the frequency regions of the PSD that correspond to the three scaling regions identified by AFA: Slow (AP: 0.027–0.186 Hz; ML: 0.026–0.193 Hz), intermediate (AP: 0.52–6.70 Hz; ML: 0.54–4.21 Hz), and fast (AP: 11.49–33.33 Hz; ML: 10.20–33.33 Hz).

particular scale has fractal dynamics, how much does it contribute to the overall spectral energy of the COP? If the majority of spectral energy of the COP can be attributed to time scales where fractal scaling is present, we could conclude that fractal scaling is an important feature of COP signals. However, if fractal scaling contributes only a small amount of spectral energy to the overall signal, then fractal scaling may not be a prominent feature and its presence should perhaps not drive efforts to model and analyze COP signals.

We calculated the fast Fourier transform (FFT) of the centered AP and ML time series using FFT length 2^{14} (= 16,384 data points) padded with zeros. We then calculated spectral power (or energy) of each frequency by squaring the amplitude associated with each FFT frequency component.[14] The total amount of power in three frequency bands, corresponding to the time scales identified below, were analyzed to determine the contribution of each scaling region to the overall signal (expressed as a percentage of total signal power contained in the three scaling regions, excluding the regions between the scaling regions).

Figure 7 illustrates the results of PSD analysis on a single trial for both AP and ML COP signals. We calculated the amount of spectral energy contained in each of the scaling regions identified by AFA and our model selection routine. The percentage of spectral energy associated with a given scale was then calculated by dividing the amount of energy at one particular scale by the total energy contained within all scaling regions (excluding the transition regions, i.e., the curved portions of the AFA plot that separated the linear scaling regions and were typically about 1–1.5 $\log_2 w$ long). Excluding the transition regions resulted in a slight overestimation of the amount of spectral energy at each scale, but enabled us to compare the relative importance of the scaling regions to each other.

Statistical Analysis

The parameters obtained from the refitted 3-region model data described above are included in all results. We averaged the values obtained from the three trials recorded from each participant for statistical analysis. In the case of the fast scaling region, we used a weighted mean since there was a variable number of trials per participant (some AFA plots did not show the first region for all three trials per participant). The weights reflected the number of trials that were averaged (from 1 to 3) to obtain the H value in the fast region for that participant. If a participant did not exhibit a fast scaling region, we did not include that participant in the analyses for H over the fast scaling region.

We used one-sample t-tests to compare the estimated H values for each identified scaling region to hypothetical means corresponding to theoretically significant boundaries (e.g., 0, 0.5, and 1) in order to characterize the scaling as reflecting antipersistent, uncorrelated (random white noise), or persistent processes.

We performed the following steps in order to perform comparisons of the lengths of the scaling regions within the same COP plane. First, we selected the subset of the data that included all three scaling regions and performed a repeated-measures analysis of variance (ANOVA) with scaling region as the sole factor on these data, and then followed with paired-samples *post hoc* t-test comparisons. Second, we used all the available data ($N = 40$) to compare only the intermediate and slow scaling regions using a paired-samples t-test.

Similarly, we performed the following steps in order to compare the H values and the length of the scaling regions across the COP planes. First, we selected a subset of the total data set that contained the fast scaling region in both the AP and ML planes and used paired-samples t-tests to compare across AP and ML for each scaling region. Second, we used all the available data to compare the AP and ML characteristics of only the intermediate and slow scaling regions using paired-samples t-tests.

We used repeated-measures ANOVA with *post hoc*, paired-samples t-tests when applicable to compare the relative contributions of the different scaling regions to the overall spectral power.

RESULTS

The mean and SD of H together with the corresponding mean and SD of the lengths of the scaling regions identified by the automated 3-region model fitting procedure are presented in Table 1 and Fig. 5.

AP COP Series

Fast Scale

There were 76 out of 115 cases that exhibited a scaling region with a length spanning only two adjacent scales; we did not consider these to be real scaling regions because they did not meet the 3-scale length criterion that we imposed for establishing the presence of fractal scaling. The scaling region in the other 39 series spanned 30–87 ms. When we averaged the H of these 39 trials (for 19 participants) we obtained $H = 0.22$ ($SD = 0.07$). One-sample weighted t-tests (using the weighting procedure described earlier) showed that H was significantly greater than 0, $t(18) = 14.35$, $p < 0.001$, and significantly less than 0.5, $t(18) = -18.85$, $p < 0.001$, indicating an anti-persistent process at the fast scale when scaling was present.

Intermediate Scale

The intermediate scaling region was identified to be 149 ms–1.91 s. Mean $H = 1.04$ ($SD = 0.10$), indicating a nonstationary, persistent process. H exceeded 1.0 for 71 of the 115 time series. However, on average, a one sample t-test showed that H was not significantly different than 1, $t(39) = 1.93$, $p = 0.06$.

Slow Scale

The slow scaling region was identified to be 5.37–37.15 s. Mean $H = 0.27$ (SD = 0.13), indicating an anti-persistent process. One sample t-tests showed that H was significantly greater than 0, $t(39) = 16.75$, $p < 0.001$, and significantly less than 0.5, $t(39) = -14.58$, $p < 0.001$.

Comparison of Scaling Region Lengths

For the subset of the participants who showed the fast scaling region for the AP COP ($N = 19$), repeated-measures ANOVA on the $\log_2 w$ lengths of the regions indicated a significant difference among the lengths of the regions, $F(1,18) = 47.06$, $p < 0.001$. *Post hoc* t-tests showed that the fast scaling region (mean = 1.49 $\log_2 w$, $SD = 0.32$) was shorter than the intermediate ($M = 3.62$ $\log_2 w$, $SD = 0.59$) and the slow (mean = 2.51 $\log_2 w$, $SD = 0.48$) regions, $t(18) = 12.95$, $p < 0.001$, and $t(18) = 6.72$, $p < 0.001$, respectively. The intermediate region was longer than the slow region for this subset of participants, $t(18) = 4.85$, $p < 0.001$. We also compared the $\log_2 w$ lengths of the intermediate and slow scaling regions for all the participants ($N = 40$) using a paired-samples t-test. This analysis also showed that the length of the intermediate scaling region (mean = 3.61 $\log_2 w$, $SD = 0.56$) was greater than the slow scaling region (mean = 2.93 $\log_2 w$, $SD = 0.64$), $t(39) = 4.27$, $p < 0.001$.

Comparison of Scaling Region Spectral Energies

There was a significant difference among the regions for the relative spectral energy they contributed in the AP plane, $F(2,78) = 1739.00$, $p < 0.001$. According to *post hoc* tests (all $p < 0.05$), the fast scaling region had the least amount of spectral energy (mean = 0.05%, $SD = 0.03$) followed by the intermediate (mean = 12.28%, $SD = 7.19$), and then slow regions (mean = 87.65%, $SD = 7.20$). The left panel of Fig. 8 portrays these results.

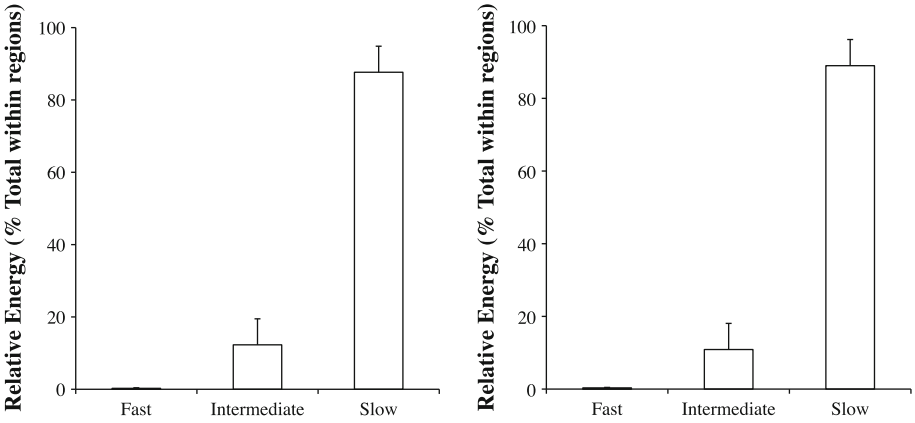

FIGURE 8. Average percentages of spectral energy associated with each scaling region identified from AFA for the slow (AP: 0.027–0.186 Hz; ML: 0.026–0.193 Hz), intermediate (AP: 0.52–6.70 Hz; ML: 0.54–4.21 Hz), and fast (AP: 11.49–33.33 Hz; ML: 10.20–33.33 Hz) scaling regions. The percentages were calculated by dividing the energy associated with a given scaling region by the total energy associated with all the defined scaling regions. Error bars depict the standard error of the mean. Most of the spectral energy in the overall COP signal is contributed by the slow time scale, with the fast time scale contributing a negligible amount and the intermediate scale also contributing very little spectral energy. Fractal scaling was most clearly defined for the intermediate scale, so the results depicted here indicate that fractal scaling was not a dominant characteristic of the COP signals.

ML COP Series

Fast Scale

There were 23 out of 115 cases with only 2-point scaling; as was the case for the AP COP, we did not consider these to be legitimate scaling regions. The scaling region in the remaining 92 series spanned 30–98 ms. When we averaged the H of these 92 trials (for 37 participants) we obtained an average $H = 0.21$ ($SD = 0.04$), indicating an anti-persistent process when scaling was present. One sample weighted t-tests showed that mean H was significantly greater than 0, $t(36) = 30.00$, $p < 0.001$, and significantly less than 0.5, $t(36) = -42.93$, $p < 0.001$.

Intermediate Scale

The intermediate scaling region was 238 ms–1.84 s. Mean $H = 1.00$ ($SD = 0.10$), indicating a persistent and borderline-nonstationary process. A total of 60 of the 115 H values were greater than 1. A one sample t-test showed that H was not significantly different from 1, $t(39) = 0.18$, $p = 0.86$.

Slow Scale

The slow scaling region was 5.19–38.75 s. Mean $H = 0.17$ ($SD = 0.06$), indicating an anti-persistent process. One sample t-tests showed that H was significantly greater than 0, $t(39) = 16.82$, $p < 0.001$, and significantly less than 0.5, $t(39) = -33.95$, $p < 0.001$.

Comparison of Scaling Region Lengths

For the subset of the data where the fast scaling region was present ($N = 37$), repeated measures ANOVA on the $\log_2 w$ lengths of the regions was significant showing that there were differences in the $\log_2$ length of the regions, $F(1,36) = 112.60$, $p < 0.001$. *Post hoc* t-tests revealed that the fast scaling region (mean = 1.68 $\log_2 w$, $SD = 0.37$) was shorter than the intermediate (mean = 2.98 $\log_2 w$, $SD = 0.40$) and the slow (mean = 2.87 $\log_2 w$, $SD = 0.41$) regions, $t(36) = 11.54$, $p < 0.001$, and $t(36) = 10.61$, $p < 0.001$, respectively. The intermediate region was not significantly different than the slow region, $t(37) = 1.16$, $p < 0.001$. We also compared the $\log_2 w$ lengths of the intermediate and slow scaling regions for all our data ($N = 40$) using a repeated-measures t-test. This analysis also showed that the $\log_2 w$ length of the intermediate scaling region (mean = 2.99 $\log_2 w$, $SD = 0.39$) was not significantly different from the slow scaling region (mean = 2.95 $\log_2 w$, $SD = 0.51$), $t(39) = 0.74$, $p = 0.32$.

Comparison of Scaling Region Spectral Energies

There was a significant difference in the relative spectral energy contributed by the scaling regions in the ML plane, $F(2,78) = 2260.00$, $p < 0.001$. According to *post hoc* tests (all $p < 0.05$), the fast scaling region had the lowest amount of spectral energy (mean = 0.12%, $SD = 0.07$) followed by the intermediate (mean = 10.88%, $SD = 6.44$) and then slow scales (mean = 88.99%, $SD = 6.45$). These results are shown in the right panel of Fig. 8.

Comparison of AP vs. ML COP Dynamics

In order to be able to compare the differences between the AP and ML COP in the fast scaling

region, we first examined the subset of the data where all three scaling regions were present in both AP and ML ($N = 18$). Paired-samples t-test showed that the fast scaling region was longer for ML (mean = 1.83 $\log_2 w$, $SD = 0.43$) than AP (mean = 1.47 $\log_2 w$, $SD = 0.10$), $t(17) = 4.03$, $p < 0.001$. The intermediate region was significantly longer for AP (mean = 3.63 $\log_2 w$, $SD =$ 0.61) than ML (mean = 2.75 $\log_2 w$, $SD = 0.39$), $t(17) = 7.24$, $p < 0.001$. The length of the slow region was not different between AP (mean = 2.53 $\log_2 w$, $SD = 0.49$) and ML (mean = 2.84 $\log_2 w$, $SD = 0.39$), $t(17) = 1.93$, $p = 0.07$. With regard to H, paired-samples t-test showed that H in the fast scaling region was greater in AP (mean = 0.22, $SD = 0.07$) than ML (mean = 0.19, $SD = 0.02$), $t(17) = 2.49$, $p = 0.02$. Paired-samples t-test showed that H for the intermediate scale did not differ between AP (mean = 1.02, $SD = 0.14$) and ML (mean = 1.01, $SD = 0.09$), $t(17) = 0.20$, $p = 0.85$. Finally, a paired-samples t-test showed that H for the slow scaling region was significantly greater for AP (mean = 0.24, $SD = 0.09$) than ML (mean = 0.19, $SD = 0.07$), $t(17) = 2.54$, $p = 0.02$.

We then analyzed data from all our participants ($N = 40$) focusing only on the intermediate and slow scaling regions. The intermediate region was significantly longer for AP (mean = 3.62 $\log_2 w$, $SD = 0.56$) than for ML (mean = 2.99 $\log_2 w$, $SD = 0.39$), $t(39) = 7.05$, $p < 0.001$. The length of the slow region was not different between the AP (mean = 2.93 $\log_2 w$, $SD = 0.64$) and ML (mean = 2.95 $\log_2 w$, $SD = 0.51$), $t(39) = -0.23$, $p = 0.81$. A paired-samples t-test showed that H for the intermediate was greater for AP (mean = 1.04, $SD = 0.14$) compared to ML (mean = 1.00, $SD = 0.10$), $t(39) = 2.08$, $p = 0.04$. H for the slow scaling region was significantly greater for AP (mean = 0.26, $SD = 0.10$) than ML (mean = 0.16, $SD = 0.06$), $t(39) = 5.81$, $p < 0.001$.

DISCUSSION

Our goal in this paper was to examine to what degree the framework of fGn–fBm processes applies to COP data during quiet stance. For an ideal fGn–fBm process one would expect to see a single scaling region. We therefore aimed to determine how many scaling regions were present in our data. We also examined the range of obtained H values in comparison to the H values expected from an ideal fractal signal in the fGn–fBm framework, which are expected to be within the range of 0–1. We discuss our findings relating to the aforementioned points with respect to the applicability of the fGn–fBm framework to the COP. Additionally, we were interested in the relative spectral energy distribution in these scaling regions to determine the extent to which fractal variability contributed to the overall COP dynamics.

Overall, a 3-region model provided the best fits to the AFA curves obtained from our COP time series. For the first (i.e., fast time scale) region, the model selection results at first seem to indicate anti-persistent fractal scaling over about 30–90 ms for some of the COP time series. However, this scaling region did not span more than two steps of 0.5 $\log_2 w$ for about 66% of the AP series and 20% of the ML time series—cases which we did not treat as reliable indications of fractal scaling. Moreover, preliminary testing of our force plate using a static weight of 45 kg revealed apparent scaling over similar time scales with an average $H = 0.18$. However, a one sample weighted t-test comparison to that H value revealed that the mean H for our COP data differed significantly from that value for both AP ($H = 0.22$) and ML ($H = 0.21$) COP series, $t(18) = 18.58$, $p < 0.001$, and $t(36) = -3.92$, $p < 0.001$, respectively. This suggests there may be processes relevant to postural control that occur on this very fast time scale, but further investigation of this issue is necessary. Scaling in this region might be related to a background state of the neuromuscular system such as muscle tension or to other, more central factors such as attention to the task.

However, there are other reasons to be quite cautious about interpreting this scaling region. It is only resolvable when sampling the COP at a relatively high rate (100 Hz in the present case), indicating the presence of a very high-frequency process (about 11–33 Hz) that contributes an almost negligible amount of spectral energy to the signal (see Fig. 8). Figure 9 shows how the scaling region is no longer resolved (but the overall form of the plot and the slopes, i.e., H values, remain unchanged) as the sampling frequency of the signal is reduced from 100 to 50 Hz and then to 25 Hz. It is important to note that while this scaling region was only revealed using the relatively high sampling rate of 100 Hz, it nevertheless does not seem to be an artifact that is caused by oversampling since its slope was different from the slope in the comparable region obtained when loading the force platform with a static weight.

An intermediate scaling region, spanning approximately 200 ms–1.9 s with H values close to 1, was reliably identified for every COP time series. This suggests a fractal process that tended to be persistent, perhaps bordering on being a nonstationary process. However, it must be noted that the time scale in question (200 ms–1.9 s, corresponding to frequencies of about 0.5–5 Hz) are rather small. As noted by Gao *et al.*,[13] the fractal scaling is occurring for portions of the signal that contain relatively little spectral energy. Our results also showed that the intermediate scaling

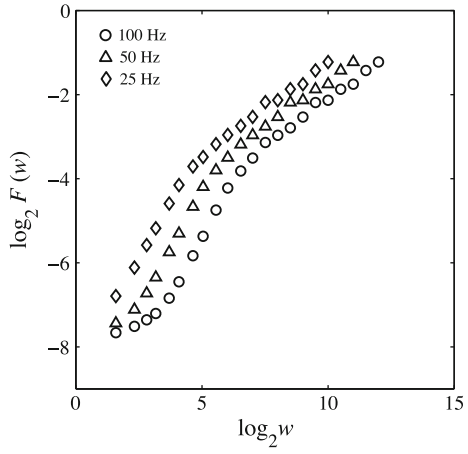

FIGURE 9. Illustration of the effects of varying the sampling rate (100, 50, and 25 Hz) on the properties of the scaling regions exhibited in the AFA plots. The slopes and $\log_2 w$ lengths of the intermediate and slow scaling regions remain constant with down-sampling, but the fast scaling region progressively disappears. This indicates that the fast scaling region is only resolvable at a relatively high sampling rate. Note that if the *x*-axis is plotted as $\log_2(w \cdot \Delta t)$, where Δt is the sampling rate, then the three curves would almost collapse onto each other.

region containing fractal dynamics only contributed approximately 11 and 12% of the overall signal energy in the AP and ML COP, respectively. The intermediate fractal scaling region was, therefore, not a dominant feature of COP dynamics.

The identification of $H \geq 1$ in the intermediate scaling region also deserves special consideration. If a given signal is truly characterized by $H > 1$, methods for which estimates of H saturate at 1 may yield erroneous results. DFA and AFA do not confront this problem, but many other fractal analysis methods saturate at $H = 1$. Besides this methodological point, we point out below the implications of $H > 1$ for modeling postural control processes.

An anti-persistent long-term (i.e., slow) scaling region, spanning about 5–40 s, was also identified. For some signals (~12% of the data) the upper limits of the region had to be manually selected because of a breakdown of fractal scaling for the largest w values. The reasons for this breakdown are at this point unclear. The results suggest a limit to the persistent long memory of COP signals. This could reflect an underlying change in the postural control strategy during the course of a trial, resulting perhaps from a shift in attention, muscular fatigue, or some other factor that leads to a very low frequency drift or oscillation of the COP.

We identified several quantitative differences between AP and ML COP signals. The fast scaling region (when present) was longer for ML than AP, while the intermediate region was significantly longer for AP than ML. In addition, H for the slow time scale was significantly greater for AP than ML, but H did not differ across AP and ML signals for the other scaling regions. Although these quantitative differences were present, overall there was qualitative similarity between the AP and ML COP signals. Both typically exhibited 3-region plots characterized by anti-persistence at the fast and slow scales and persistence in the intermediate scale. The similarities suggest a similar overall style of control over AP and ML postural sway, while the observed quantitative differences may relate to musculoskeletal factors that clearly differ across the two planes of motion (e.g., greater range of motion for AP, different sets of muscles involved in motion in the two planes, etc.,).

Further Implications for Postural Control

These findings raise important questions about the fundamental nature of COP signals and about the kinds of models and methods best suited for understanding postural control. Foremost among these issues is the strong possibility that the framework of fGn–fBm processes[11] may not apply to COP signals. Several of our findings suggest this is the case. If the COP was an ideal fBm process, we would expect to observe only one scaling region with H values ranging between 0 and 1. Our data indicate the existence of at least 2 (and potentially 3) scaling regions in the COP. We also observed that in 62% of the AP trials and 52% of the ML trials H in the intermediate region exceeded 1, the theoretical upper limit for fBm. In addition, the presence of the curved segments of the AFA plots, especially for large $\log_2 w$, is also inconsistent with the fBm model. Finally, another observation that is inconsistent with the fGn–fBm model is the typically observed under-additivity of slopes found when comparing results from non-integrated and integrated COP signals. A fBm process can be obtained by integrating a fGn process, so the difference in H values for two such signals should differ by exactly 1.[12] For COP signals, however, the difference is usually less than 1 (for example, see Table 1 in Delignières *et al.*[7]). Along these lines, it is also important to emphasize that H values will be different if COP data are treated as random walk process or as an increment process.

Taken together, these findings indicate that other model frameworks beyond the fGn–fBm model should be considered for understanding postural control. We propose that the COP might usefully be characterized from the framework of models of ON/OFF intermittency. There are several features of our data consistent with the properties of an ON/OFF process. Just over half of our time series exhibited $H > 1$ over the inter-

mediate scale. ON/OFF intermittency can produce $H \geq 1$ as shown previously in the context of some relatively simple mathematical systems that can produce ON/OFF intermittency.[12,14] In addition, the mean H for the fast time scale was nearly identical to the mean H for the slow time scale. It is possible that the two scaling regions both result from the same intermittent process, such as the presence of occasional, large, discontinuous shifts in the COP. These occasional ON periods could affect the fast scaling region because each shift is effectively instantaneous, and simultaneously affect the slow scaling region because the amount of time between these events (OFF periods) is typically large.

The presence of fine-grained, anti-persistent fluctuations at the fast scaling region is also compatible with the idea of noisy COP fluctuations occurring about a moving set point. Moving set-point models have an ON/OFF-intermittency interpretation (although they may not have initially been framed in this way). One such model is the rambling-trembling hypothesis of Zatsiorsky and Duarte.[35] The hypothesis states that postural control during quiet stance results from hierarchical control with two levels: The highest level specifies the reference position for maintaining equilibrium, while the lower level maintains balance around that reference position by negating deviations (''trembling'') from it. The set point for equilibrium migrates (''rambles'') during quiet stance. This scheme is consistent with ON/OFF intermittency because if the COP is not at the set point then restoring force corrections are enacted to keep the body in equilibrium (corresponding to an ''ON'' state); if it is on the set point, then the COP is left unchecked (corresponding to an ''OFF'' state). A similar idea was also advanced by Dijkstra[9] in his moving set-point model, in which fine-grained fluctuations occur about a moving equilibrium point.

Another previous finding consistent with ON/OFF intermittency models is the presence of small, occasional, ballistic contractions of the gastrocnemius and soleus muscles during quiet stance.[22] These movements occur at a rate of about 2.6 times per single displacement of the center of mass and apparently serve to limit center of mass movement. The active, ballistic corrections within this framework correspond to the ''ON'' state, while the periods when sway is left uncorrected correspond to the ''OFF'' state. The OFF states may also be related to the existence of a ''proprioceptive dead zone'' stemming from the inability of muscle mechanoreceptors to resolve changes in ankle angle less than 0.5°; while in the dead zone, muscle activity is mostly absent.[21]

Limitations

This study represents an initial effort to apply AFA to COP signals. The study did not include any experimental manipulations, and thus based on these results we cannot make any claims about the sensitivity of AFA to changes in COP dynamics. It will be useful in future studies to identify the sensitivity of AFA to the effects of sensory factors (e.g., the availability of vision), task factors (e.g., concurrent performance of a cognitive or manual task), or individual factors (e.g., expertise or pathology). Another need that becomes apparent when evaluating the results of this study is to examine the factors that contribute to the many individual differences in the findings, for example between the fast scaling region fits. There is also a need to develop more objective criteria for choosing many of the analysis parameters, as currently many steps require a judgment call. While these judgments can be enhanced by familiarity with one's dataset they remain fundamentally subjective. In addition, further scrutiny of the fast scaling region is warranted. Finally, we identified features of the data consistent with ON/OFF intermittency, but at this point the similarities are somewhat superficial and the evidence is very preliminary. We plan to further investigate the suitability of this framework for characterizing and understanding COP signals in future modeling and empirical studies.

Conclusions

The results suggest that the fGn–fBm framework may not be adequate for modeling and characterizing COP signals. The identification of multiple scaling regions and the possibility that ON/OFF intermittency could produce the observed COP dynamics (i.e., $H > 1$ for the intermediate scaling region) furthermore suggests that multiscale approaches (e.g., scale-dependent Lyapunov exponents or multifractal analyses)[12,14] may be valuable for characterizing COP data, especially for capturing the low-frequency components of the COP which are responsible for the majority of the spectral energy in the signal.

ACKNOWLEDGMENTS

This research was supported by NSF grants CMMI 1031958 (JG) and BCS 0926662 (MAR).

REFERENCES

[1]Bardet, J.-M., and P. Bertrand. Identification of the multiscale fractional Brownian motion with biomechanical applications. *J. Time Series Anal.* 28:1–52, 2007.

[2]Beran, J. Statistics for Long-Memory Processes. Boca Raton, FL: CRC Press, 319 pp, 1994.

[3]Blázquez, M. T., M. Anguiano, F. Arias de Saavedra, A. M. Lallena, and P. Carpena. Study of the human postural control system during quiet standing using detrended fluctuation analysis. *Physica A* 388:1857–1866, 2009.

[4]Collins, J. J., and C. J. De Luca. Open-loop and closed-loop control of posture: a random-walk analysis of center-of-pressure trajectories. *Exp. Brain Res.* 95:308–318, 1993.

[5]Collins, J. J., and C. J. De Luca. Random walking during quiet standing. *Phys. Rev. Lett.* 73:764–767, 1994.

[6]Davids, K., S. Bennett, and K. M. Newell. Movement System Variability. Champaign, IL: Human Kinetics, 376 pp, 2006.

[7]Delignières, D., K. Torre, and P. L. Bernard. Transition from persistent to anti-persistent correlations in postural sway indicates velocity-based control. *PLoS Comput. Biol.* 7(2):e1001089, 2011. doi:10.1371/journal.pcbi.1001089.

[8]Delignières, D., T. Deschamps, A. Legros, and N. Caillou. A methodological note on non-linear time series analysis: is Collins and De Luca (1993)'s open- and closed-loop model a statistical artifact? *J. Motor Behav.* 35:86–96, 2003.

[9]Dijkstra, T. M. H. A gentle introduction to the dynamic set-point model of human postural control during perturbed stance. *Hum. Mov. Sci.* 19:567–595, 2000.

[10]Duarte, M., and V. M. Zatsiorksy. Long-range correlations in human standing. *Phys. Lett. A* 283:124–128, 2001.

[11]Eke, A., P. Hermán, J. Bassingthwaighte, G. Raymond, D. Percival, M. Cannon, I. Balla, and C. Ikrényi. Physiological time series: distinguishing fractal noises from motions. *Pflug Arch. Eur. J. Phys.* 439:403–415, 2000.

[12]Gao, J. B., J. Hu, W. W. Tung, Y. H. Cao, N. Sarshar, and V. P. Roychowdhury. Assessment of long range correlation in time series: how to avoid pitfalls. *Phys. Rev. E* 73: 016117, 2006.

[13]Gao, J. B., J. Hu, and W. W. Tung. Facilitating joint chaos and fractal analysis of biosignals through nonlinear adaptive filtering. *PLoS ONE* 6(9):e24331, 2011. doi:10.1371/journal.pone.0024331.

[14]Gao, J. B., Y. H. Cao, W. W. Tung, and J. Hu. Multiscale Analysis of Complex Time Series—Integration of Chaos and Random Fractal Theory, and Beyond. Hoboken, NJ: Wiley, 368 pp, 2007.

[15]Gao, J., J. Hu, T. Buckley, K. White, and C. Hass. Shannon and Renyi entropies to classify effects of mild traumatic brain injury on postural sway. *PLoS ONE* 6(9):e24446, 2011. doi:10.1371/journal.pone.0024446.

[16]Gao, J., J. Hu, X. Mao, and M. Perc. Culturomics meets random fractal theory: insights into long-range correlations of social and natural phenomena over the past two centuries. *J. R. Soc. Interface*, 2012. doi:10.1098/rsif.2011.0846.

[17]Gao, J. B., H. Sultan, J. Hu, and W. W. Tung. Denoising nonlinear time series by adaptive filtering and wavelet shrinkage: a comparison. *IEEE Signal Proc. Lett.* 17:237–240, 2010.

[18]Harbourne, R. T., and N. Stergiou. Movement variability and the use of nonlinear tools: principles to guide physical therapist practice. *Phys. Ther.* 89:267–282, 2009.

[19]Hu, J., J. B. Gao, and X. S. Wang. Multifractal analysis of sunspot time series: the effects of the 11-year cycle and Fourier truncation. *J. Stat. Mech.*:P02066, 2009.

[20]Lin, D., H. Seol, M. A. Nussbaum, and M. L. Madigan. Reliability of COP-based postural sway measures and age-related differences. *Gait Posture* 28:337–342, 2008.

[21]Loram, I. D., M. Lakie, I. Di Giulio, and C. N. Maganaris. The consequences of short-range stiffness and fluctuating muscle activity for proprioception of postural joint rotations: the relevance to human standing. *J. Neurophysiol.* 102:460–474, 2009.

[22]Loram, I. D., C. N. Maganaris, and M. Lakie. Human postural sway results from frequent, ballistic bias impulses by soleus and gastrocnemius. *J. Physiol.* 654:295–311, 2005.

[23]Mandelbrot, B. B. Fractals and Scaling in Finance. New York: Springer, 1997.

[24]Mandelbrot, B. B., and J. W. van Ness. Fractional Brownian motions, fractional noises and applications. *SIAM Rev.* 10:422–437, 1968.

[25]McQuarrie, A. D. A small-sample correction for the Schwarz SIC model selection criterion. *Stat. Probab. Lett.* 44:79–86, 1999.

[26]Minamisawa, T., K. Takakura, and T. Yamaguchi. Detrended fluctuation analysis of temporal variation of the center of pressure (COP) during quiet standing in Parkinsonian patients. *J. Phys. Ther. Sci.* 21:287–292, 2009.

[27]Peng, C. K., S. V. Buldyrev, S. Havlin, S. M. Simons, H. E. Stanley, and A. L. Goldberger. Mosaic organization of DNA nucleotides. *Phys. Rev. E* 49:1685–1689, 1994.

[28]Riley, M. A., R. Balasubramaniam, S. Mitra, and M. T. Turvey. Visual influences on the center of pressure dynamics of upright posture. *Ecol. Psychol.* 10:65–92, 1998.

[29]Riley, M. A., R. Balasubramaniam, and M. T. Turvey. Recurrence quantification analysis of postural fluctuations. *Gait Posture* 11:12–24, 1999.

[30]Riley, M. A., and M. T. Turvey. Variability and determinism in motor behavior. *J. Motor Behav.* 34:99–125, 2002.

[31]Seidel, D. J., and J. R. Lazante. An assessment of three alternatives to linear trends for characterizing global atmospheric temperature changes. *J. Geophys. Res.* 109: 1–10, 2004. doi:10.1029/2003JD004414.

[32]Tung, W. W., J. B. Gao, J. Hu, and L. Yang. Detecting chaos in heavy noise environments. *Phys. Rev. E* 83:046210, 2011.

[33]van Emmerik, R. E. A., and E. E. H. van Wegen. On variability and stability in human movement. *J. Appl. Biomech.* 16:394–406, 2000.

[34]Winter, D. A. Biomechanics and Motor Control of Human Movement. Hoboken, NJ: John Wiley and Sons, 325 pp, 2005.

[35]Zatsiorsky, V. M., and M. Duarte. Rambling and trembling in quiet standing. *Motor Control* 4:185–200, 2000.